

# Transit Timing and Duration Variations for the Discovery and Characterization of Exoplanets

Eric Agol and Daniel C. Fabrycky

**Abstract** Transiting exoplanets in multi-planet systems have non-Keplerian orbits which can cause the times and durations of transits to vary. The theory and observations of transit timing variations (TTV) and transit duration variations (TDV) are reviewed. Since the last review, the *Kepler* spacecraft has detected several hundred perturbed planets. In a few cases, these data have been used to discover additional planets, similar to the historical discovery of Neptune in our own Solar System. However, the more impactful aspect of TTV and TDV studies has been characterization of planetary systems in which multiple planets transit. After addressing the equations of motion and parameter scalings, the main dynamical mechanisms for TTV and TDV are described, with citations to the observational literature for real examples. We describe parameter constraints, particularly the origin of the mass/eccentricity degeneracy and how it is overcome by the high-frequency component of the signal. On the observational side, derivation of timing precision and introduction to the timing diagram are given. Science results are reviewed, with an emphasis on mass measurements of transiting sub-Neptunes and super-Earths, from which bulk compositions may be inferred.

## Introduction

Transit Timing Variations (TTV) and Transit Duration Variations (TDV) are two of the newest tools in the exoplanetary observer's toolbox for discovering and characterizing planetary systems. Like most such tools, they rely on indirect inferences,

---

Eric Agol

Department of Astronomy, Box 351580, University of Washington, Seattle, WA 98195-1580, USA  
e-mail: agol@uw.edu

Daniel C. Fabrycky

Dept. of Astronomy & Astrophysics, University of Chicago, Chicago, IL 60637, USA e-mail:  
fabrycky@uchicago.edu

rather than detecting light from the planet directly. However, the amount of dynamical information they encode is extremely rich.

To decode this information, let us start with the dynamical concepts. Consider the vector stretching from the star of mass  $m_0$  to the planet of mass  $m$  to be  $\mathbf{r} = (x, y, z)$ , with a distance  $r$  and direction  $\hat{\mathbf{r}}$ . The Keplerian potential per reduced mass,  $\phi = -GM/r$  (where  $M \equiv m_0 + m$  and the planet is replaced with a body of reduced mass  $\mu \equiv m_0 m / M$ ), gives rise to closed orbits. This means that, in the absence of perturbations, the trajectory is strictly periodic,  $\mathbf{r}(t + P) = \mathbf{r}(t)$ . Moreover, Kepler showed that Tycho Brahe’s excellent data for planetary positions were consistent with Copernicus’ idea of a heliocentric system only if the planets (including the Earth) followed elliptical paths of semi-major axis  $a$ , and one focus on the Sun. Newton was successful at finding the principle underlying such orbits, a force law  $\mathbf{F} = \mu \ddot{\mathbf{r}} = -G\mu m_0 r^{-2} \hat{\mathbf{r}}$ , which results in a period  $P = 2\pi a^{3/2} (GM)^{-1/2}$  (i.e. with the  $a$ -scaling Kepler found the planets actually obeyed).

This research program was thrown into some doubt by the “Great Inequality,” the fact that the orbits of Jupiter and Saturn did not fit the fixed Keplerian ellipse model. This obstacle was overcome by the perturbation theory of Laplace, who used the masses derived via their satellite orbits to explain the deviations of their heliocentric orbits (Wilson 1985). The insight can be calculated by writing an additional force to that of gravity of the Sun:

$$\mathbf{F}_1 = -G\mu_1 M r_1^{-2} \hat{\mathbf{r}}_1 + \mathbf{F}_{12}, \quad (1)$$

where now the forces and distances specifically pertains to planet 1, and a force of planet 2 on planet 1 is added. This latter force consists of two terms:

$$\mathbf{F}_{12} = \mu_1 \ddot{\mathbf{r}}_1 = G\mu_1 m_2 |r_2 - r_1|^{-3} (\mathbf{r}_2 - \mathbf{r}_1) - G\mu_1 m_2 r_2^{-2} \hat{\mathbf{r}}_2. \quad (2)$$

The first term on the right-hand-side is the direct gravitational acceleration of planet 1 due to planet 2. The second is an indirect frame-acceleration effect, due to the acceleration the star feels due to the second planet. Since the Sun is fixed at the zero of the frame, this acceleration is modelled by acceleration of planet 1 in the opposite direction.

Likewise, Leverrier and Adams used planet-planet perturbations in the first discovery of a planet by gravitational means (Adams 1847; Le Verrier 1877). In this case, they did not know the zeroth order solution (i.e. the Keplerian ellipse) for the perturber, Neptune. In its place, they assumed the Titius-Bode rule held, and sought only the phase of the orbit. This technique worked because they only wanted to see how the acceleration, then deceleration, of Uranus as it passed Neptune, would betray Neptune’s position on the sky to optical observers. The task of discovering planets by TTV is more demanding. We do not have any hints as to what the planet’s orbit might be, i.e. we cannot assume it is on a circular orbit or obeys some spacing law. The observation of a single orbit is insufficient for a detection: times of least three transits are needed to measure a period change. However, due to measurement error, in only a small fraction of cases is the high-frequency “chopping” signal (see Chopping section below) statistically significant after just three transits. Moreover,

the sampling of the orbit only at transit phase causes aliasing of the dynamical signals.

The times of transit are primarily constrained by the decline of stellar flux during transit ingress, and the rise over egress, which occur on a timescale

$$\tau \approx \pi^{-1} P (R_p/a) \approx 2.2 \text{min} \left( \frac{R_p}{R_\oplus} \right) \left( \frac{M_\star}{M_{\text{sun}}} \right)^{-1/3} \left( \frac{P}{10\text{d}} \right)^{1/3}, \quad (3)$$

assuming a circular orbit, edge-on to the line of sight (impact parameter of  $b = 0$ ), around a star of mass  $M_\star$ ; usually timing precision can be measured to better than this timescale. This timing precision gives a sensitive measure of the variation of the angular position of a planet relative to a Keplerian orbit. In contrast, the other dynamical techniques rely on a signal spread through the orbital timescale  $P$ , and thus the precision of the orbital phase is poorly constrained unless the measurements are of high precision or long duration (although these conditions have been achieved by pulsar timing in PSR 1257 +12 which detected a Great Inequality (Wolszczan 1994) and by radial velocity in GJ 876 which detected resonant orbital precession (Laughlin and Chambers 2001)).

Orbital positions or transit times are expressed in a table called an ephemeris. Perturbations cause motions or timing deviations from a Keplerian reference model, especially changes to its instantaneous semimajor axis  $a$ , eccentricity  $e$ , and longitude of periastron  $\omega$ . The latter angle is between the position of closest approach and a plane perpendicular to the line of sight that contains either the primary body or the center of mass. In the case of transit timing variations, the Keplerian alternative is simply an ephemeris with a constant transit period,  $P$ :

$$C = T_0 + P \times E, \quad (4)$$

where  $E$  is the epoch – an integer transit number – and  $T_0$  is the time of the transit numbered  $E = 0$ ;  $C$  stands for “calculated” based on a constant-period model. Meanwhile, the Observed times of transit are denoted  $O$ . This notation leads to an  $O - C$  (pronounced “O minus C”; Sterken 2005) diagram, in which only the perturbation part is plotted. An instructive version, modelled after the timing of WASP-47 (Becker et al. 2015) but with a greatly exaggerated perturbation, is shown in figure 1. The transit times come earlier than the linear model for transit numbers 0-3 and 11-14, and later than the linear model for transit numbers 4-10. These deviations from a constant transit period are what we call TTVs.

The other dynamical effect addressed by this review is TDVs. Like TTVs, the cause can be changes in  $a$ ,  $e$ , or  $\omega$ . The most dramatic effect, however, is due to orbital plane reorientation. The angle the orbital plane’s normal vector makes to the observer’s line of sight — the inclination,  $i$  — determines the length of the transit chord. Changes in the inclination will change the length of that chord, which in turn changes the amount of time the planet remains in transit: duration variations.

The literature on exoplanets has a history of rediscovering effects that had been well studied in the field of binary and multiple stars. In the current focus, it has long

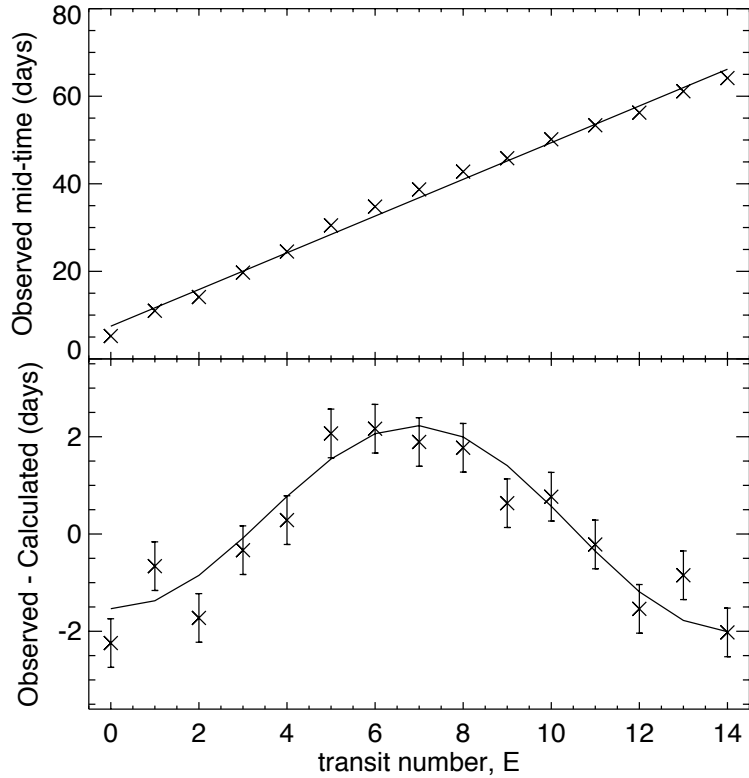


**Fig. 1** An example of timing data. *Top panel:* the measured midtimes of exoplanet transits, to which a line is fit by least-squares. *Bottom panel:* the residuals of that fit, which is the conventional observed minus calculated ( $O - C$ ) diagram; the original sinusoidal function, to which Gaussian noise was added, is also plotted as a line.

been known to eclipsing-binary observers that long-term depth changes can result from the torque of a third star orbiting the pair (Mayer 1971). This effect owes to the secular and tidal dynamics which dominate triple star systems (Borkovits et al. 2003), dictated by their hierarchical configuration which allows them to remain stable. TDV due to perturbing planets is simply its exoplanetary analogue (Miralda-Escudé 2002).

The first recognition of the importance of transit timing and duration variations was at the DPS and AAS meetings two decades ago by Dobrovolskis and Borucki (1996a,b), followed a few years later by Miralda-Escudé (2002) and Schneider (2003, 2004). More detailed studies that included the important effect of mean-motion resonance, in which the ratio of two planets' orbital periods is close to the ratio of small integers, were independently investigated by Holman and Murray (2005) and Agol et al. (2005). The former paper showed that Solar-system like perturbations might be used to find Earth-like planets, should transit times be measured

with sufficient accuracy. The latter paper coined the term ‘transit-timing variations,’ with acronym TTV, and defined TTVs as the observable accumulation of transit period changes (i.e.  $O - C$ ).

Initial studies of TTVs of hot Jupiters were able to place limits on the presence of Earth-mass planets near mean-motion resonance (Steffen and Agol 2005). Some further studies claimed detection of perturbing planets causing TTVs or TDVs, but each of these were quickly disputed or refuted by additional measurements. The first convincing detection awaited the launch of the *Kepler* spacecraft, and the discovery of Kepler-9 which showed large-amplitude TTVs of two Saturn-sized planets with strong significance (Holman et al. 2010); this discovery was remarkably similar to predictions based upon the GJ 876 system (Agol et al. 2005). The Kepler-9 paper kicked off a series of discoveries of TTVs with the *Kepler* spacecraft, with now more than 100 systems displaying TTVs, and a handful showing TDVs (Holczer et al. 2016).

## Preliminaries

Since the gravitational interactions between planets occur on the orbital timescale, the amplitude of TTVs is proportional to the orbital period of each planet, times a function of other dimensionless quantities. Thanks to Newton’s second law and Newton’s law of gravity, the acceleration of a body does not depend on its own mass. Thus, the TTVs of each planet scale with the masses of the *other* bodies in the system. In a two-planet system, then, to lowest order in mass ratio, the  $O - C$  formulae are:

$$\begin{aligned}\delta t_1 &= P_1 \frac{m_2}{m_0} f_{12}(\alpha_{12}, \theta_{12}), \\ \delta t_2 &= P_2 \frac{m_1}{m_0} f_{21}(\alpha_{12}, \theta_{21}),\end{aligned}\tag{5}$$

where the masses of the star and planets are  $m_0, m_1$ , and  $m_2$ , and  $f_{ij}$  describes the perturbations of planet  $j$  on planet  $i$ , which is a function of the semi-major axis ratio,  $\alpha_{ij} = \min(a_i/a_j, a_j/a_i)$ , and the angular orbital elements of the planets,  $\theta_{ij} = (\lambda_i, e_i, \omega_i, I_i, \Omega_i, \lambda_j, e_j, \omega_j, I_j, \Omega_j)$ . The evaluation of these functions can be found in a series of papers on perturbation theory: Nesvorný and Morbidelli (2008); Nesvorný (2009); Nesvorný and Beaugé (2010); Agol and Deck (2016); Deck and Agol (2016).

With the addition of multiple perturbing planets, if the mass-ratios of the planets to the star are sufficiently small and if none of the pairs of planets are in a mean-motion resonance, then the TTVs may be approximately expressed as linear combinations of the perturbations due to each companion. For  $N$  planets, the TTVs become

$$\delta t_i = P_i \sum_{j \neq i} \frac{m_j}{m_0} f_{ij}(\alpha_{ij}, \theta_{ij}),\tag{6}$$

for  $i = 1, \dots, N$ .

The largest TTVs are caused by orbital period changes associated with librations of the system about a mean-motion resonance. Energy trades can be used to compute the amplitude of the TTV in each planet (see Agol et al. 2005; Holman et al. 2010). Because of Kepler's relation  $a \propto P^{3/2}$ , a period lengthening of  $\delta P_1 \ll P_1$  is associated with a semi-major axis change of  $\delta a_1 = (3/2)a_1 \delta P_1 / P_1$ . Differentiating the orbital energy equation  $E_1 = -GMm_1/(2a_1)$  shows that such a change results in an energy change of  $\delta E_1 = (GMm_1 a_1^{-2}/2)\delta a_1$ . To conserve total energy, the other planet will have an energy change of  $\delta E_2 = -(GMm_1 a_1^{-2}/2)\delta a_1$ , which can also be expressed as  $+(GMm_2 a_2^{-2}/2)\delta a_2$ . Using the relation  $\delta a_2 = (3/2)a_2 \delta P_2 / P_2$ , and the Keplerian relation  $a_2/a_1 = (P_2/P_1)^{2/3}$ , we obtain:

$$\delta P_2 = -\delta P_1 (m_1/m_2) (P_2/P_1)^{5/3}. \quad (7)$$

When considering the  $O-C$  shapes that each planet makes over a fixed time interval (e.g. from a survey that measures transits for both planets), we will have a factor of  $P_2/P_1$  more orbital periods for the inner planet than the outer planet. Thus the accumulated time shift of the signal,  $\delta t$ , builds up more for the inner planet, by one factor of the period ratio. In consideration of equation 7, we are left with:

$$\delta t_2 = -\delta t_1 (m_1/m_2) (P_2/P_1)^{2/3}. \quad (8)$$

This scaling agrees with analytic work performed in the resonant (Nesvorný and Vokrouhlický 2016) and near-resonant (Lithwick et al. 2012; Hadden and Lithwick 2016) regimes. Hence the TTV curves of the two planets are anti-correlated, with the ratio of planetary masses determining the ratio of TTV amplitudes. In the case that the masses are equal, the amplitude of the outer planet's TTV is larger because its orbital size needs to change more for its Keplerian orbital energy to equal the change in the inner planet's Keplerian orbital energy.

In general, transit timing variations afford a means of measuring the density of exoplanets. The two observables associated with a light curve are the time stamp of each photometric measurement and the number of photons measured. The number of photons is a dimensionless number, and thus may only constrain dimensionless quantities, such as radius ratio, impact parameter, or the ratio of the stellar size to the semi-major axis. The quantities that have units of time — the period, transit duration, ingress duration — can constrain the density of the system since the dynamical time relates to stellar density,  $\rho$ , as  $t_{dyn} \approx (G\rho)^{-1/2}$ . Seager and Mallén-Ornelas (2003) showed that a single transiting planet on a well-measured circular orbit may be used to gauge the density of the star; in the case of multiple transiting planets, the circular assumption may be relaxed (Kipping 2014).

The transit depth, then, gives the radius-ratio of the planet to the star, while if two planets transit and show TTVs, their TTVs give an estimate of the mass ratio of the perturbing planet to the star. Thus, two transiting, interacting planets yield an estimate of the density ratio of the planets to the star, and consequently we can obtain the density of the planets. Note that this is true even if the absolute mass and

radius of the star are poorly constrained. A caveat to this technique is that there is an eccentricity dependence that is present in the stellar density estimate. However, multi-transiting planet systems typically require low eccentricities to be stable, and in some cases the eccentricities can be constrained sufficiently from TTV analysis, from analyzing multiple planets (Kipping 2014), or from statistical analysis of an ensemble of planets (Hadden and Lithwick 2017). So this caveat ends up not impacting the stellar density estimate significantly (the mass-eccentricity degeneracy, however, reduces precision on planet-star mass ratios, and hence inflates the planet density uncertainty). Another way to obtain an estimate of stellar density is from asteroseismology: in fact, the time-dependence of asteroseismic measurements is what enables density to be constrained in that case as well (Ulrich 1986).

If a pair of transiting exoplanets can be detected with *both* TTVs and RVs, then the absolute dimensions of the system may be obtained (Agol et al. 2005; Montet and Johnson 2013) as RVs have dimensions of velocity, which when combined with time measurements from TTVs gives dimensions of distance. In practice this technique has yet to yield useful constraints upon the properties of planetary systems (Almenara et al. 2015), but it may prove fruitful in the future much as double-lined spectroscopic binaries have used to measuring the properties of binary stars, as hinted at by Almenara et al. (2016). Circumbinary planets (CBP) are an extreme example of this technique: the timing offsets of the transits, combined with the eclipses and radial-velocity of the binary give very precise constraints on the absolute parameters of the Kepler-16 system (Doyle et al. 2011).

## Theory and Paradigmatic Examples

Here we discuss the physical models for different types of TTV interactions, and point the reader to real systems that exhibit each kind of interaction.

Close to resonances, a combination of changes in semi-major axis and eccentricity lead to TTV cycles whose period depends on the separation from the resonance (Steffen 2006; Lithwick et al. 2012); the latter refer to this as the ‘super-period.’ The main TTV variation comes from only one resonance, the one the system is closest to, which allows its critical angles to move slowly and thus its effect to build up. If the period ratio  $P_2/P_1$  is within a few percent of the ratio  $j/k$ , with  $j$  and  $k$  being integers, then the expected TTV period is

$$P_{\text{TTV}} = 1/|j/P_2 - k/P_1|. \quad (9)$$

The order of the resonance is  $|j - k|$ , and the strength of the resonance depends on the planetary eccentricities to a power of the order minus 1. Therefore, first order resonances affect planets with no initial eccentricity, but higher order resonances have a large effect only in the presence of some eccentricity.

Seeing two planets transit the star helps immensely to characterize a near-resonant system, because then the relative transit phase of the two planets can be

compared with the phase of the TTV signals (Lithwick et al. 2012). If the eccentricities are maximally damped out, then the resonant terms of the interaction continue forcing a small eccentricity that quickly precesses, causing the TTV. In that case, the phase of the signal is predictable, and the two planets' eccentricities are anti-aligned, so the TTV signals consist of anti-correlated sinusoids. Also useful in that case is that the amplitudes lead directly to the planetary masses. If so-called "free eccentricity" remains, however, the phases would usually differ from that prediction, the TTV in the two planets may not be in perfect anti-phase, and only an approximate mass scale rather than a measurement is available, which is referred to as the mass-eccentricity degeneracy. The first real system that showed this pattern convincingly was Kepler-18 (Cochran et al. 2011). The degeneracy between mass and eccentricity results from sampling at the period of the transiting planet, which causes short period variations to be aliased with  $P_{TTV}$  (Lithwick et al. 2012; Deck and Agol 2015).

The measurement of TTVs and TDVs has been used for confirmation, detection, and characterization of transiting exoplanets and their companions. The *Kepler* spacecraft discovered thousands of transiting exoplanet candidates; the classification as 'candidate' was cautiously used to allow for other possible explanations, such as a blend of a foreground star and a background eclipsing binary causing an apparent transit-like signal. The presence of multiple transiting planets around the same star gave a means of confirming two planets that display *anti-correlated* TTVs: due to energy conservation (equation 8), the anti-correlation indicates dynamical interactions between the two planets, while such a configuration would not be stable for a triple star system. Many papers used this technique to confirm that *Kepler* planet candidates were bonafide exoplanets using different techniques to identify the anticorrelation in data (Ford et al. 2012a,b; Fabrycky et al. 2012; Steffen et al. 2012; Xie 2013).

The characterization of exoplanets with TTVs also began in earnest with the *Kepler* spacecraft. In addition to Kepler-9, the Kepler-18 system was characterized by a combination of TTVs and RVs, giving density estimates for the three transiting planets (Cochran et al. 2011) and assuring that the new method for mass characterization gave the same answers as the trusted, older method.

When only one planet transits in a near-resonant system, the measured TTVs may simply record a sinusoidal signal, which could result from the other planet being close to many different resonances with the transiting planet (Meschiari and Laughlin 2010). In Kepler-19, Ballard et al. (2011) were able to tell that a planetary companion was the only sensible cause of the TTV, but they were not able to break this finite set of degeneracies.

This degeneracy has made it extremely difficult to characterize non-transiting planets via TTV, and hence in many cases an additional planet is suspected due to TTV, but detailed work has not been pursued to determine its nature. The first case of a non-transiting planet being discovered *and* completely characterized was Kepler-46 (a.k.a. KOI-872; Nesvorný et al. 2012). The authors found that the TTVs of the transiting planet were far from a sinusoidal shape; in fact, they could be Fourier-decomposed into at least four significant sinusoids. Each of these sinusoids can be



identified as the interaction with the non-transiting planet via a different resonance. Even with all this extra information, TTVs could only narrow down the possible perturbing planets to a degenerate set of two, and below we describe how TDVs broke this degeneracy.

Planets that are truly in resonance with each other have the largest TTV signals. On a medium-baseline timescale like that of *Kepler*, they can perturb each other's orbital periods. The resonant interaction traps the planets at a specific period ratio, causing the periods to oscillate near that ratio. The period of the full cycle of that oscillation depends on the ratio of the planet masses to the host star's mass, to the  $-2/3$  power (Agol et al. 2005; Nesvorný and Vokrouhlický 2016). For instance, the touchstone system GJ876 has a 550 day libration cycle, about 10 times the outer planet's period, due to its relatively massive planets and low-mass star. A system which was characterized by resonant interaction is KOI-142 (Nesvorný et al. 2013), in which a non-transiting planet was discovered. A system with two transiting planets in resonance with large TTVs is Kepler-30 (Fabrycky et al. 2012). A system with smaller libration amplitudes, but a surprising *four* planets in resonance (forming a chain of resonances) is Kepler-223 (Mills et al. 2016).

Several other TTV mechanisms have been detected which do not rely on resonances, but are relevant for more hierarchical situations ( $P_2/P_1 \gtrsim 4$ ).

If the outer planet transits, and the inner orbiting body is very massive, the dominant effect can be the shifting of the primary star with respect to the barycenter. Then, as the outer planet orbits the barycenter, it arrives at the moving target either early or late. This effect was numbered (i) by Agol et al. (2005), and it is seen clearly in circumbinary planet systems. For instance, the secondary star of Kepler-16 (Doyle et al. 2011) moves the primary by many times its own radius, resulting in an  $\sim 8$  day TTV on top of a 225 day orbit.

A final mechanism of dynamical TTV is relevant for the inner orbit when a massive body orbits at large distance. The tide that body exerts on the inner orbit causes its orbital period to differ slightly from what it would be in the absence of that outer body. If the outer body is in the plane of the inner orbit, its tide slows down the inner orbit, lengthening its period. If the outer body is far out of the plane of the inner orbit, its tide speeds up the inner orbit, shortening its period. The tide also depends on the third power of the distance to that external body. Hence, when the external body moves on an eccentric and/or inclined orbit, it induces a period variation in the inner orbit, which has the period of the outer orbit. Also important for the timing is how the outer perturber instantaneously torques the inner orbit's eccentricity. These effects were put together and analyzed by Borkovits et al. (2003) in the context of triple star systems, and the in-plane physics was explained as mechanism (ii) of Agol et al. (2005). An example of these effects was provided by Kepler-419 (Dawson et al. 2014), in which an eccentric massive planet accompanies an inner planet with a period ratio of 9.7.

## ***Chopping***

When two planets are nearly resonant, the degeneracy between the mass ratios of the planets to the star and the eccentricity vector may be broken by examining additional TTV components present in the data (Deck and Agol 2015). Non-resonant perturbations occur on the time from one conjunction of the planets to the next, which is when their separation is smallest and gravitational attraction is strongest. Conjunctions occur on a period of  $P_{\text{syn}} = (1/P_1 - 1/P_2)^{-1}$ , also referred to as the synodic period. TTVs at the synodic period, and its harmonics, have smaller amplitude due to the fact that they do not add coherently, and thus require higher signal-to-noise to detect. These synodic variations are referred to as “chopping” as they commonly show TTVs that alternate early and late, on top of the larger amplitude TTVs with period  $P_{TTV}$ . Despite the smaller amplitude, the chopping components can be detected in many cases, and can break the mass-eccentricity degeneracy, leading to a unique measurement of the masses of the exoplanets (Nesvorný and Vokrouhlický 2014; Schmitt et al. 2014; Deck and Agol 2015).

As an example, consider a pair of planets with period ratio of  $P_2/P_1 = 1.52$ . This period ratio is close to 3:2, and thus is affected by this resonant term, giving a TTV period of  $38P_1$  by equation 9. Figure 2 compares two planets with this period ratio with zero eccentricity and mass-ratios of  $10^{-6}$  to a pair of planets with eccentricities of  $e_1 = e_2 = 0.04$  and mass-ratios near  $10^{-7}$ . Both pairs of planets give nearly identical amplitudes for the large resonant term due to the mass-eccentricity degeneracy discussed above, while the larger mass ratio planets show a much stronger chopping variation. In this case there is a clear difference between the TTVs of the two simulated systems: the inner planet shows a drift over three orbital periods, and a sudden jump every third orbital period, while the outer one shows a similar pattern over two orbital periods. In this example the phase of the orbital parameters are set such that the TTV amplitudes match; change in the phase can also be indicative of a non-zero eccentricity contributing to the TTVs, and with an ensemble of planets which are believed to have a similar eccentricity distribution, the mass-eccentricity degeneracy may be broken statistically (Lithwick et al. 2012; Hadden and Lithwick 2014).

## ***Transit Duration Variations***

TDVs have given useful results for characterization of individual systems, though fewer in number than TTVs. Three mechanisms for TDV have been observed in planetary system orbiting a single primary star.

The first is torque due to the rotational oblateness of the star. It is a convincing model for the duration changes in Kepler-13 b (KOI 13.01 Szabó et al. 2012) and a controversial explanation for transit shape anomalies in PTFO 8-8695 (Barnes et al. 2013).

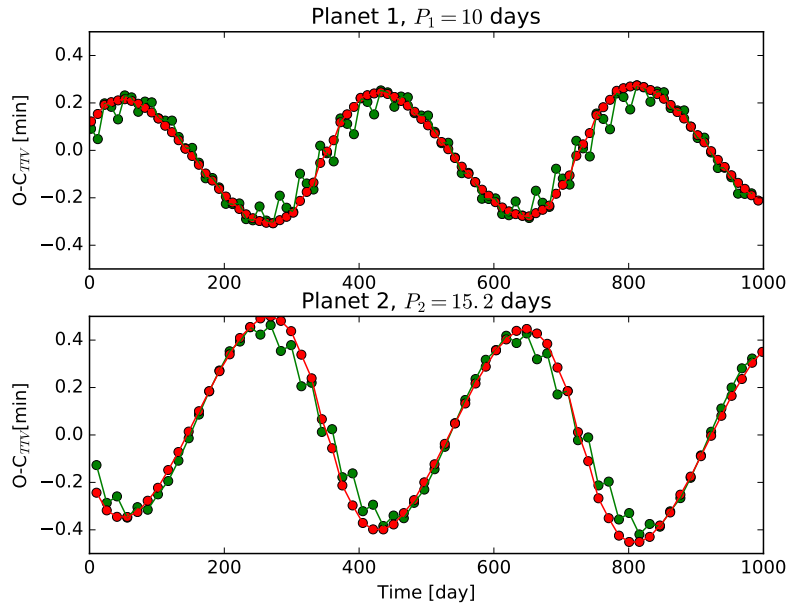


**Fig. 2** Transit-timing variations of two low-eccentricity planets with larger mass ratios,  $m_1 = m_2 = 10^{-6}m_*$  (green) compared with two higher eccentricity planets ( $e_1 = e_2 = 0.04$ ) with smaller mass ratios  $m_1 = m_2 = 10^{-7}m_*$ . The zig-zag chopping component is apparent in the high-mass/low-eccentricity case, while less apparent in the low-mass/ high-eccentricity case.

The second planetary cause of TDVs is eccentricity variations due to a resonant interaction. The length of the chord across the star, as well as the speed at which the planet moves along that chord, are changed during the planetary interaction. This effect has been observed in KOI-142 (Nesvorný et al. 2013). Slow, secular precession of the eccentricity is expected by general relativity (Pál and Kocsis 2008), by stellar oblateness (Heyl and Gladman 2007), and by tidal distortion (Ragozzine and Wolf 2009), but these mechanisms have not given rise to observable TDV to date, for planets around single stars. It is likely that very long time-baseline measurements, or comparing the measurements of two time-separated space missions like Kepler and Plato, will be able to detect this effect.

The third cause of TDVs for planets around single stars is inclination changes due to secular precession of the orbital plane. Torques from other planets were observed in Kepler-117 (Almenara et al. 2015) and Kepler-108 (Mills and Fabrycky 2017), the latter indicating mutual inclination of  $\sim 15^\circ$  in a rather hierarchical pair of planets.

Earlier the case of Kepler-46 was described, in which TTV measurements of a transiting planet led to two degenerate possibilities for the identity of an additional, non-transiting, planet. The clever resolution (Nesvorný et al. 2012) was to note that in one of those solutions, to get the relative amplitudes of the component sinusoids correct in the TTV signal, the perturbing planet must be somewhat inclined with respect to the transiting planet. As a consequence, a torque on that planet would

drive TDV. No such TDV were observed, so the unique solution — which is at a different orbital period and planetary mass, and closer to coplanar — was found.

Extending this inclination mechanism of TDV to two stars and a planet, the precession of circumbinary planets (CBPs) has been so extreme as to cause transits to turn on and off (Martin 2017). This observation is similar to the several known cases of stellar triples with inner sometimes-eclipsing binaries, but in this case it is most observable in the outer orbit. The first case of that phenomenon was Kepler-35 (Welsh et al. 2012), and the most spectacular observed so far is Kepler-413 (Kostov et al. 2014), in which a  $4^\circ$  mutual inclination caused transits to stop and then start again nearly half a precession cycle later.

Additional dramatic TDVs can occur in CBP systems due to the moving-target effect described above for TTVs. If the transit occurs while the star is moving in the same direction as the planet, the transit duration is longer; if in opposite directions, the transit duration is shorter. Matching the prediction from the phase of the binary completely secures the interpretation of the signal that an object is in a circumbinary orbit, as discussed extensively by Kostov et al. (2013) for the cases of Kepler-47 and Kepler-64 (a.k.a. PH-1, KIC 4862625b).

## Observational considerations: timing precision

The steepest portions of a transit are the ingress and egress when the planet crosses onto and off of the disk of the star, causing a dip of depth  $\delta = (R_p/R_*)^2$  if limb-darkening is ignored. Suppose for the moment that the only source of noise is Poisson noise due to the count rate of the star,  $\dot{N}$ . The photometric uncertainty over the duration of ingress,  $\tau$  (eqn. 3), scales as  $(\dot{N}\tau)^{1/2}$ . If the time of ingress fit from a model is offset by  $\sigma_\tau$ , then the difference in counts observed versus the model is  $\sigma_\tau\delta\dot{N}$  (the pink region in Fig. 3). Equating this count deficit to the photometric uncertainty gives  $\sigma_\tau = \tau^{1/2}\dot{N}^{-1/2}\delta^{-1}$ , which is the 68.3% confidence timing precision assuming that the exposure time is much shorter than the ingress duration and that  $\sigma_\tau \ll \tau$ . The same formula applies to egress. A longer transit ingress duration leads to a shallower slope in ingress, which makes it more difficult to measure an offset in time of the model. Higher count rates and deeper transits improve the precision, as expected. Note that we've assumed that the duration of the transit is sufficiently long that the error on  $\delta$  is small.

Suppose the transit duration is  $T$ . Then, the uncertainty on the duration is given by the sum of the uncertainties on the ingress and egress, added in quadrature:  $\sigma_T = \sqrt{2}\sigma_\tau$ . The timing precision,  $\sigma_t$ , is set by the mean of the ingress and egress, giving  $\sigma_t = \frac{1}{\sqrt{2}}\sigma_\tau$ .

A more complete derivation of these expressions is given by Carter et al. (2008), while an expression which includes the effects of a finite integration time is given by Price and Rogers (2014). The assumptions of no limb-darkening and Poisson noise are generally broken by stars; in addition, stellar variability contributes to timing uncertainty, for which there is yet to be a general expression. These effects gen-

erally increase the uncertainty on the measurement of transit times and durations, and so the best practice would be to estimate the timing uncertainties from the data, accounting for effects of correlated stellar variability by including the full covariance matrix of the timing uncertainty (Carter and Winn 2009; Gibson et al. 2012; Foreman-Mackey et al. 2017). Crossing of the path of the planet across star spots may also cause some uncertainty on the timing precision (Oshagh et al. 2013; Barros et al. 2013); this can be diagnosed by a larger scatter within transit than outside transit or other signs of significant stellar activity, and can be handled best by including the spots in the transit model (Ioannidis et al. 2016).

Note that the barycentric light-travel time offset must be corrected for carefully for high-precision TTV (Eastman et al. 2010).

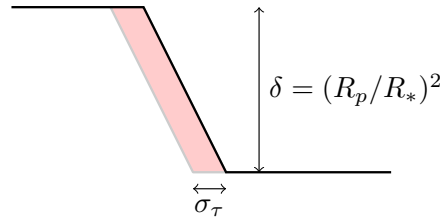


**Fig. 3** Diagram of the transit ingress of a planet, flux versus time. The precision of the timing of ingress,  $\sigma_\tau$ , is set by when the area of the ingress (pink) equals the timing precision over the duration of ingress. The same applies to egress, albeit with the time flipped in this plot.

## Science Results

The best characterized pair of small planets to date using TTV reside in the Kepler-36 system (Carter et al. 2012). As this planet pair is in close proximity, the conjunctions cause a significant kick to each planet resulting a TTV amplitude that is  $\approx 1\%$  of the orbital periods of the planets. Figure 4 shows a ‘river-plot’ for all seventeen quarters of long-cadence *Kepler* data for this pair of planets. After each 7(6) orbits of the inner(outer) planet (or so), there is a conjunction which causes a change in the eccentricity vector and period of each planet. The change in the eccentricity vector causes a sudden change in the subsequent transit time, while the change in period causes a change in slope; these are apparent for Kepler-36c in Figure 4. The large TTVs enable a precise measurement of the planet-star mass ratios for both planets (using the TTVs of the companion planet), while the star shows asteroseismic variability which gives a precise estimate of the stellar mass. The result are masses with uncertainties of  $< 8\%$ , which is the most precise to date for planets of approximately this mass or lower,  $4.5 \pm 0.3$  and  $8.1 \pm 0.6 M_\oplus$ . The inner planet shows a density which is consistent with scaling up in mass a planet of the composition of

Earth, while the outer planet requires a significant H/He envelope to explain its size which is comparable to Neptune (Carter et al. 2012).

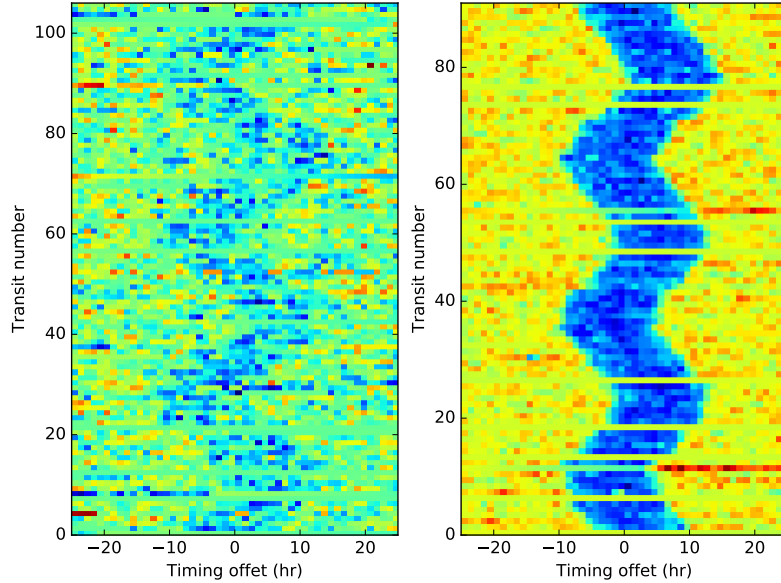


**Fig. 4** River plot of Kepler-36b (left) and Kepler-36c (right). Each row of each panel shows the intensity of the star scaled with color and centered on the mean ephemeris of each planet.

A wide-spread phenomenon was detected by TTV characterization of masses: the existence of puffy sub-Neptune planets. In the first such case, Kepler-11 e (Lissauer et al. 2011), a planet with a mass half of Neptune’s has a size slightly bigger than Neptune. Even more extreme cases of this class have been found, the most extreme which we consider secure is a  $2.1^{+1.5}_{-0.8} M_{\oplus}$  planet with a radius of  $7R_{\oplus}$  in Kepler-51 (Masuda 2014). These massive envelopes mean these low-mass planets formed while gas was still present in the protoplanetary disk, and that they were able to capture that gas, a surprising result (e.g. Lee and Chiang 2016; Ginzburg et al. 2016).

Catalogs of transit times have been produced for the multi-planet *Kepler* systems (Mazeh et al. 2013; Rowe et al. 2015; Holczer et al. 2016). Several analyses of an ensemble of TTV pairs of planets have recently been carried out (Hadden and Lithwick 2014; Xie 2013, 2014; Jontof-Hutter et al. 2016), with the largest by Hadden & Lithwick (2016), yielding constraints on the RMS eccentricity of the population of planets. A slightly smaller sample, selecting only planets with mass precisions of better than  $3 - \sigma$ , yields Figure 5. There appears to be a trend of mean density decreasing with orbital period (one exception is K2-3d, although the authors warn its RV mass estimate may be affected by stellar variability). At periods near  $\approx 10$  days, the RV and TTV densities agree rather well. At shorter period, most of the RV detections are single-planets, which in general appear to have lower density relative to

their multi-planet counterparts (Steffen 2016; Mills and Mazeh 2017). When radius is plotted versus mass, and color-coded as a function of flux, Fig. 5, there is a general trend of radius increasing with mass, albeit with a large scatter in mass, while a handful of ‘puffy’ planets (with masses measured with TTV) show shockingly large radii given their small masses. These mass measurements are surprising, but difficult to dispute as larger masses would have led to a larger, and hence easier-to-measure, TTV signal.

With the end of the primary *Kepler* mission, the data volume of transit times has diminished. Nevertheless, the K2 mission has continued to provide TTV systems such as WASP-47, the first short-period hot Jupiter with nearby planet companions (Becker et al. 2015). The surprising discovery of seven planets orbiting a late-type star, TRAPPIST-1, also displays significant TTVs which will be used to precisely characterize the densities of these small exoplanets (Gillon et al. 2017). With the launch of TESS in 2018 (Ricker et al. 2015), transit timing will enhance the analysis of the multi-planet systems found, especially near the polar regions with longer term coverage, or when followed up with CHEOPS (Beichman et al. 2014). The PLATO mission next decade will cause another spike in TTV science (Rauer et al. 2014), as will possibly WFIRST (Montet et al. 2017). The James Webb Space Telescope may allow the extension in time baseline and increase in precision for high-priority transit-timing targets (Beichman et al. 2014). All to say, the future of characterizing multi-transiting planet systems with TTV (and TDVs) looks promising.

**Acknowledgements** EA acknowledges support from NASA Grants NNX13AF20G, NNX13A124G, NNX13AF62G, from National Science Foundation (NSF) grant AST-1615315, and from NASA Astrobiology Institute’s Virtual Planetary Laboratory, supported by NASA under cooperative agreement NNH05ZDA001C. DCF acknowledges support from NASA under Grant No. NNX14AB87G issued through the *Kepler* Participating Scientist Program and from the Alfred P. Sloan Foundation. We thank Sam Hadden, Jack Lissauer, Kento Masuda, Mahmoudreza Oshagh, and Jason Steffen for feedback, and we thank the Other Worlds Laboratory at UC Santa Cruz for hospitality while revising this paper.

## References

- Adams JC (1847) An Explanation of the Observed Irregularities in the Motion of Uranus, on the Hypothesis of Disturbances caused by a more Distant Planet; with a Determination of the Mass, Orbit, and Position of the Disturbing Body. *MmRAS*16:427
- Agol E Deck K (2016) Transit Timing to First Order in Eccentricity. *ApJ*18:177
- Agol E, Steffen J, Sari R Clarkson W (2005) On detecting terrestrial planets with timing of giant planet transits. *MNRAS*359:567–579
- Almenara JM, Díaz RF, Mardling R et al. (2015) Absolute masses and radii determination in multiplanetary systems without stellar models. *MNRAS*453:2644–2652
- Almenara JM, Díaz RF, Bonfils X Udry S (2016) Absolute densities, masses, and radii of the WASP-47 system determined dynamically. *A&A*595:L5
- Ballard S, Fabrycky D, Fressin F et al. (2011) The Kepler-19 System: A Transiting 2.2 R<sub>⊕</sub> Planet and a Second Planet Detected via Transit Timing Variations. *ApJ*743:200

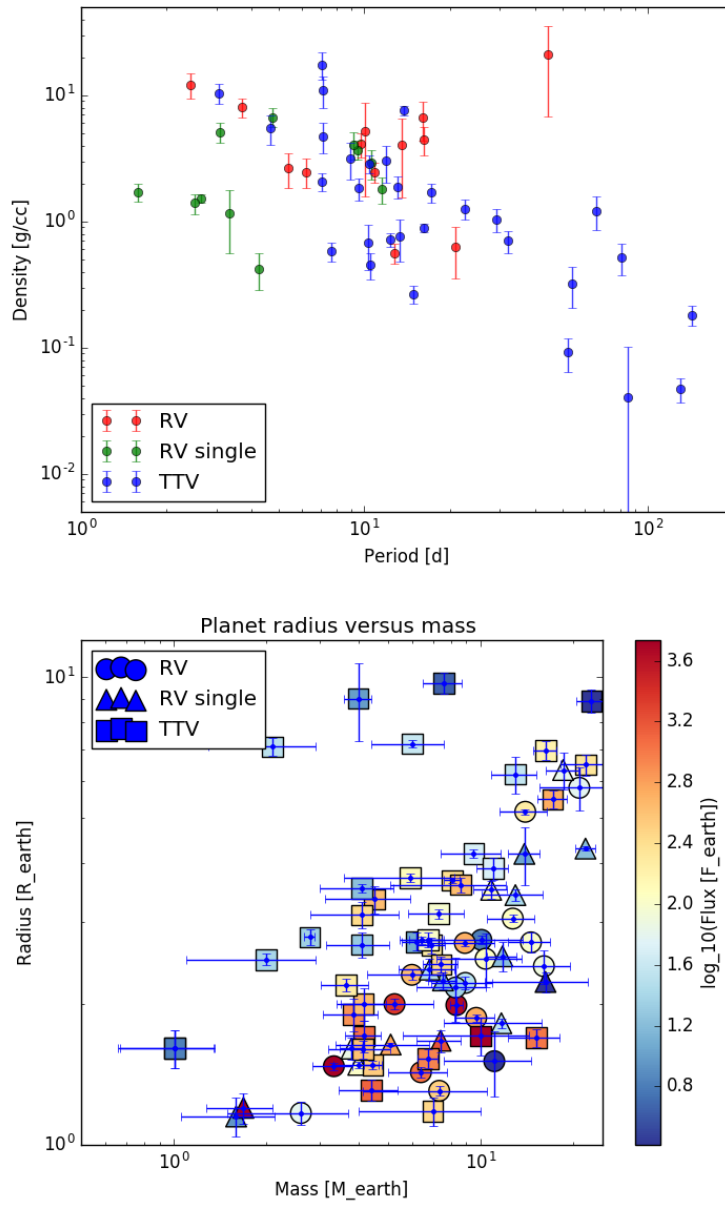


**Fig. 5** Density vs. period for planets transiting planets with masses  $< 25M_{\oplus}$  (left). Radius vs. mass, with color indicating incident stellar flux (right).



- Barnes JW, van Eyken JC, Jackson BK, Ciardi DR Fortney JJ (2013) Measurement of Spin-orbit Misalignment and Nodal Precession for the Planet around Pre-main-sequence Star PTFO 8-8695 from Gravity Darkening. *ApJ*774:53
- Barros SCC, Boué G, Gibson NP et al. (2013) Transit timing variations in WASP-10b induced by stellar activity. *MNRAS*430:3032–3047
- Becker JC, Vanderburg A, Adams FC, Rappaport SA Schwengeler HM (2015) WASP-47: A Hot Jupiter System with Two Additional Planets Discovered by K2. *ApJ*812:L18
- Beichman C, Benneke B, Knutson H et al. (2014) Observations of Transiting Exoplanets with the James Webb Space Telescope (JWST). *PASP*126:1134–1173
- Borkovits T, Érdi B, Forgács-Dajka E Kovács T (2003) On the detectability of long period perturbations in close hierarchical triple stellar systems. *A&A*398:1091–1102
- Carter JA Winn JN (2009) Parameter Estimation from Time-series Data with Correlated Errors: A Wavelet-based Method and its Application to Transit Light Curves. *ApJ*704:51–67
- Carter JA, Yee JC, Eastman J, Gaudi BS Winn JN (2008) Analytic Approximations for Transit Light-Curve Observables, Uncertainties, and Covariances. *ApJ*689:499-512
- Carter JA, Agol E, Chaplin WJ et al. (2012) Kepler-36: A Pair of Planets with Neighboring Orbits and Dissimilar Densities. *Science* 337:556
- Cochran WD, Fabrycky DC, Torres G et al. (2011) Kepler-18b, c, and d: A System of Three Planets Confirmed by Transit Timing Variations, Light Curve Validation, Warm-Spitzer Photometry, and Radial Velocity Measurements. *ApJS*197:7
- Dawson RI, Johnson JA, Fabrycky DC et al. (2014) Large Eccentricity, Low Mutual Inclination: The Three-dimensional Architecture of a Hierarchical System of Giant Planets. *ApJ*791:89
- Deck KM Agol E (2015) Measurement of Planet Masses with Transit Timing Variations Due to Synodic “Chopping” Effects. *ApJ*802:116
- Deck KM Agol E (2016) Transit Timing Variations for Planets near Eccentricity-type Mean Motion Resonances. *ApJ*821:96
- Dobrovolskis AR Borucki WJ (1996a) Influence of Jovian Extrasolar Planets on Transits of Inner Planets. In: AAS/Division for Planetary Sciences Meeting Abstracts #28, Bulletin of the American Astronomical Society, vol 28, p 1112
- Dobrovolskis AR Borucki WJ (1996b) Influence of Jovian extrasolar planets on transits of inner planets. In: Bulletin of the American Astronomical Society, BAAS, vol 28, p 1112
- Doyle LR, Carter JA, Fabrycky DC et al. (2011) Kepler-16: A Transiting Circumbinary Planet. *Science* 333:1602
- Eastman J, Siverd R Gaudi BS (2010) Achieving Better Than 1 Minute Accuracy in the Heliocentric and Barycentric Julian Dates. *PASP*122:935–946
- Fabrycky DC, Ford EB, Steffen JH et al. (2012) Transit Timing Observations from Kepler. IV. Confirmation of Four Multiple-planet Systems by Simple Physical Models. *ApJ*750:114
- Ford EB, Fabrycky DC, Steffen JH et al. (2012a) Transit Timing Observations from Kepler. II. Confirmation of Two Multiplanet Systems via a Non-parametric Correlation Analysis. *ApJ*750:113
- Ford EB, Ragozzine D, Rowe JF et al. (2012b) Transit Timing Observations from Kepler. V. Transit Timing Variation Candidates in the First Sixteen Months from Polynomial Models. *ApJ*756:185
- Foreman-Mackey D, Agol E, Angus R Ambikasaran S (2017) Fast and scalable Gaussian process modeling with applications to astronomical time series. *ArXiv e-prints*
- Gibson NP, Aigrain S, Roberts S et al. (2012) A Gaussian process framework for modelling instrumental systematics: application to transmission spectroscopy. *MNRAS*419:2683–2694
- Gillon M, Triaud AHMJ, Demory BO et al. (2017) Seven temperate terrestrial planets around the nearby ultracool dwarf star TRAPPIST-1. *Nature*542:456–460
- Ginzburg S, Schlichting HE Sari R (2016) Super-Earth Atmospheres: Self-consistent Gas Accretion and Retention. *ApJ*825:29
- Hadden S Lithwick Y (2014) Densities and Eccentricities of 139 Kepler Planets from Transit Time Variations. *ApJ*787:80
- Hadden S Lithwick Y (2016) Numerical and Analytical Modeling of Transit Timing Variations. *ApJ*828:44

- Hadden S Lithwick Y (2017) Kepler planet masses and eccentricities from TTV analysis. *The Astronomical Journal* 154(1):5, URL <https://doi.org/10.3847/1538-3881/aa71ef>
- Heyl JS Gladman BJ (2007) Using long-term transit timing to detect terrestrial planets. *MNRAS* 377:1511–1519
- Holzer T, Mazeh T, Nachmani G et al. (2016) Transit Timing Observations from Kepler. IX. Catalog of the Full Long-cadence Data Set. *ApJS* 225:9
- Holman MJ Murray NW (2005) The Use of Transit Timing to Detect Terrestrial-Mass Extrasolar Planets. *Science* 307:1288–1291
- Holman MJ, Fabrycky DC, Ragozzine D et al. (2010) Kepler-9: A System of Multiple Planets Transiting a Sun-Like Star, Confirmed by Timing Variations. *Science* 330:51
- Ioannidis P, Huber KF Schmitt JHMM (2016) How do starspots influence the transit timing variations of exoplanets? Simulations of individual and consecutive transits. *A&A* 585:A72
- Jontof-Hutter D, Ford EB, Rowe JF et al. (2016) Secure Mass Measurements from Transit Timing: 10 Kepler Exoplanets between 3 and 8  $M_{\oplus}$  with Diverse Densities and Incident Fluxes. *ApJ* 820:39
- Kipping DM (2014) Characterizing distant worlds with asterodensity profiling. *MNRAS* 440:2164–2184
- Kostov VB, McCullough PR, Hinse TC et al. (2013) A Gas Giant Circumbinary Planet Transiting the F Star Primary of the Eclipsing Binary Star KIC 4862625 and the Independent Discovery and Characterization of the Two Transiting Planets in the Kepler-47 System. *ApJ* 770:52
- Kostov VB, McCullough PR, Carter JA et al. (2014) Kepler-413b: A Slightly Misaligned, Neptune-size Transiting Circumbinary Planet. *ApJ* 784:14
- Laughlin G Chambers JE (2001) Short-Term Dynamical Interactions among Extrasolar Planets. *ApJ* 551:L109–L113
- Le Verrier UJ (1877) Tables du mouvement de Neptune fondees sur la comparaison de la theorie avec les observations. *Annales de l’Observatoire de Paris* 14:1
- Lee EJ Chiang E (2016) Breeding Super-Earths and Birthing Super-puffs in Transitional Disks. *ApJ* 817:90
- Lissauer JJ, Fabrycky DC, Ford EB et al. (2011) A closely packed system of low-mass, low-density planets transiting Kepler-11. *Nature* 470:53–58
- Lithwick Y, Xie J Wu Y (2012) Extracting Planet Mass and Eccentricity from TTV Data. *ApJ* 761:122
- Martin DV (2017) Circumbinary planets - II. When transits come and go. *MNRAS* 465:3235–3253
- Masuda K (2014) Very Low Density Planets around Kepler-51 Revealed with Transit Timing Variations and an Anomaly Similar to a Planet-Planet Eclipse Event. *ApJ* 783:53
- Mayer P (1971) Eclipsing variable IU Aurigae. *Bulletin of the Astronomical Institutes of Czechoslovakia* 22:168
- Mazeh T, Nachmani G, Holzer T et al. (2013) Transit Timing Observations from Kepler. VIII. Catalog of Transit Timing Measurements of the First Twelve Quarters. *ApJS* 208:16
- Meschiari S Laughlin GP (2010) Systemic: A Testbed for Characterizing the Detection of Extrasolar Planets. II. Numerical Approaches to the Transit Timing Inverse Problem. *ApJ* 718:543–550
- Mills SM Fabrycky DC (2017) Kepler-108: A mutually inclined giant planet system. *The Astronomical Journal* 153(1):45, URL <http://stacks.iop.org/1538-3881/153/i=1/a=45>
- Mills SM Mazeh T (2017) The Planetary Mass-Radius Relation and Its Dependence on Orbital Period as Measured by Transit Timing Variations and Radial Velocities. *ApJ* 839:L8
- Mills SM, Fabrycky DC, Migaszewski C et al. (2016) A resonant chain of four transiting, sub-Neptune planets. *Nature* 533:509–512
- Miralda-Escudé J (2002) Orbital Perturbations of Transiting Planets: A Possible Method to Measure Stellar Quadrupoles and to Detect Earth-Mass Planets. *ApJ* 564:1019–1023
- Montet BT Johnson JA (2013) Model-independent Stellar and Planetary Masses from Multi-transiting Exoplanetary Systems. *ApJ* 762:112

- Montet BT, Yee JC Penny MT (2017) Measuring the Galactic Distribution of Transiting Planets with WFIRST. *PASP*129(4):044,401
- Nesvorný D (2009) Transit Timing Variations for Eccentric and Inclined Exoplanets. *ApJ*701:1116–1122
- Nesvorný D Beaugé C (2010) Fast Inversion Method for Determination of Planetary Parameters from Transit Timing Variations. *ApJ*709:L44–L48
- Nesvorný D Morbidelli A (2008) Mass and Orbit Determination from Transit Timing Variations of Exoplanets. *ApJ*688:636–646
- Nesvorný D Vokrouhlický D (2014) The Effect of Conjunctions on the Transit Timing Variations of Exoplanets. *ApJ*790:58
- Nesvorný D Vokrouhlický D (2016) Dynamics and Transit Variations of Resonant Exoplanets. *ApJ*823:72
- Nesvorný D, Kipping DM, Buchhave LA et al. (2012) The Detection and Characterization of a Nontransiting Planet by Transit Timing Variations. *Science* 336:1133
- Nesvorný D, Kipping D, Terrell D et al. (2013) KOI-142, The King of Transit Variations, is a Pair of Planets near the 2:1 Resonance. *ApJ*777:3
- Oshagh M, Santos NC, Boisse I et al. (2013) Effect of stellar spots on high-precision transit light-curve. *A&A*556:A19
- Pál A Kocsis B (2008) Periastron precession measurements in transiting extrasolar planetary systems at the level of general relativity. *MNRAS*389:191–198
- Price EM Rogers LA (2014) Transit Light Curves with Finite Integration Time: Fisher Information Analysis. *ApJ*794:92
- Ragozzine D Wolf AS (2009) Probing the Interiors of very Hot Jupiters Using Transit Light Curves. *ApJ*698:1778–1794
- Rauer H, Catala C, Aerts C et al. (2014) The PLATO 2.0 mission. *Experimental Astronomy* 38:249–330
- Ricker GR, Winn JN, Vanderspek R et al. (2015) Transiting Exoplanet Survey Satellite (TESS). *Journal of Astronomical Telescopes, Instruments, and Systems* 1(1):014003
- Rowe JF, Coughlin JL, Antoci V et al. (2015) PLANETARY CANDIDATES OBSERVED BYKEPLER. v. PLANET SAMPLE FROM q1–q12 (36 MONTHS). *The Astrophysical Journal Supplement Series* 217(1):16, URL <https://doi.org/10.1088/0067-0049/217/1/16>
- Schmitt JR, Agol E, Deck KM et al. (2014) Planet Hunters. VII. Discovery of a New Low-mass, Low-density Planet (PH3 C) Orbiting Kepler-289 with Mass Measurements of Two Additional Planets (PH3 B and D). *ApJ*795:167
- Schneider J (2003) Multi-planet system detection by transits. In: Combes F, Barret D, Contini T Pagani L (eds) *SF2A-2003: Semaine de l’Astrophysique Française*, p 149
- Schneider J (2004) Multi-planet system detection with Eddington. In: Favata F, Aigrain S Wilson A (eds) *Stellar Structure and Habitable Planet Finding*, ESA Special Publication, vol 538, pp 407–410
- Seager S Mallén-Ornelas G (2003) A Unique Solution of Planet and Star Parameters from an Extrasolar Planet Transit Light Curve. *ApJ*585:1038–1055
- Steffen J (2006) Detecting new planets in transiting systems. PhD thesis, University of Washington
- Steffen JH (2016) Sensitivity bias in the mass–radius distribution from transit timing variations and radial velocity measurements. *Mon Not R Astron Soc* 457(4):4384–4392, URL <http://dx.doi.org/10.1093/mnras/stw241>
- Steffen JH Agol E (2005) An analysis of the transit times of TrES-1b. *MNRAS*364:L96–L100
- Steffen JH, Fabrycky DC, Ford EB et al. (2012) Transit timing observations from Kepler - III. Confirmation of four multiple planet systems by a Fourier-domain study of anticorrelated transit timing variations. *MNRAS*421:2342–2354
- Sterken C (2005) The O-C Diagram: Basic Procedures. In: Sterken C (ed) *The Light-Time Effect in Astrophysics: Causes and cures of the O-C diagram*, *Astronomical Society of the Pacific Conference Series*, vol 335, p 3

- Szabó GM, Pál A, Derekas A et al. (2012) Spin-orbit resonance, transit duration variation and possible secular perturbations in KOI-13. *Monthly Notices of the Royal Astronomical Society: Letters* 421(1):L122–L126, URL <https://doi.org/10.1111/j.1745-3933.2012.01219.x>
- Ulrich RK (1986) Determination of stellar ages from asteroseismology. *ApJ*306:L37–L40
- Welsh WF, Orosz JA, Carter JA et al. (2012) Transiting circumbinary planets Kepler-34 b and Kepler-35 b. *Nature*481:475–479
- Wilson C (1985) The Great Inequality of Jupiter and Saturn: from Kepler to Laplace. *Archive for History of Exact Sciences* 33:15–290
- Wolszczan A (1994) Confirmation of Earth-Mass Planets Orbiting the Millisecond Pulsar PSR B1257+12. *Science* 264:538–542
- Xie JW (2013) Transit Timing Variation of Near-resonance Planetary Pairs: Confirmation of 12 Multiple-planet Systems. *ApJS*208:22
- Xie JW (2014) Transit Timing Variation of Near-resonance Planetary Pairs. II. Confirmation of 30 Planets in 15 Multiple-planet Systems. *ApJS*210:25